International Journal of Environmental Sciences
ISSN: 2229-7359
Vol. 11 No. 4,2025
https://theaspd.com/index.php

Electrochemical And Thermal Characterization Of The Li-NCM NM3100 Cell For EV Applications

Saravanan Sivasamy[1], Vinod S[2], Balaji M[3], Rudhra S[4], Prabhu S[5]
[1]Department of Electrical and Electronics Engineering, SRM Institute of Science and Technology, Ramapuram, Cennai 600089, Tamil Nadu, India
[2]Department of Electrical and Electronics Engineering, Jerusalem College of Engineering, Anna University, Chennai 600100, Tamil Nadu, India.
[3]Department of Electrical and Electronics Engineering, Sri Sivasubramaniya Nadar College of Engineering, Kalavakkam 603110, Tamil Nadu, India.
[4]Department of Electrical and Electronics Engineering, Jerusalem College of Engineering, Anna University, Chennai 600100, Tamil Nadu, India.
[5]Department of Electrical and Electronics Engineering, Mohan babu University, A. Rangampeta, Tirupati 517102, Andhra Pradesh, India.
sarantajmahal@gmail.com, vinod@jerusalemengg.ac.in, balajim@ssn.edu.in, rudhra@jerusalemengg.ac.in, prabhutajmahal6@gmail.com,

Abstract
This study presents a detailed evaluation of the Li-NCM NM3100 battery cell, focusing on its electrochemical behavior, thermal stability, and aging characteristics under electric vehicle (EV)-relevant operating conditions. The cell demonstrates excellent thermal performance, with temperature variations restricted to approximately 0.03 °C, and maintains a low ohmic resistance in the range of 0.0042 to 0.0046 Ω·m². These factors indicate effective internal heat management and robust electrode integrity, both critical for high-power EV applications. Throughout the discharge process, the state of charge (SOC) decreases gradually from 100% to approximately 1.8%, delivering a cumulative capacity of 2.88 Ah and an energy output of 10.52 Wh. This smooth decline, without any sharp voltage drops, reflects strong coulombic efficiency and consistent energy delivery. The discharge voltage remains stable, with a plateau extending from approximately 4.20 V to 2.72 V, averaging around 3.42 V, highlighting efficient energy utilization. Even under repeated cycling, the cell retains over 90% of its capacity, confirming long-term durability and resistance to performance fade. Further analysis of differential capacity (dQ/dV) curves reveals progressive shifts and broadening of intercalation peaks and troughs, which are linked to solid electrolyte interphase (SEI) growth and lithium trapping—two key aging mechanisms in lithium-ion batteries. Overall, the NM3100 cell exhibits a highly stable thermal and electrochemical profile, high efficiency, and predictable aging patterns. These results make it a strong candidate for integration into next-generation EV battery systems where performance, safety, and longevity are paramount.

Keywords: *Electric Vehicles (EVs), Lithium-ion Batteries (LIBs), State of Charge (SOC), Thermal Management, Energy Efficiency, Voltage Characteristics, Capacity Retention, Battery Aging Processes.*

INTRODUCTION

The Li-NCM NM3100 battery cell represents a significant advancement in lithium-ion technology, tailored specifically for the growing demands of modern electric vehicles (EVs). Built on a robust lithium-nickel-cobalt-manganese (NCM) chemistry, this cell strikes a well-considered balance between energy density, power output, safety, and longevity. At its core, the NM3100 leverages a highly refined NCM cathode formulation that enables high specific capacity, translating into extended vehicle driving range and more efficient energy utilization (Hammou et al., 2023). This makes it a compelling choice for EV manufacturers striving to enhance both performance and practicality. One of the standout features of the NM3100 is its improved thermal stability(Prabhu S et al., 2025), which plays a vital role in minimizing the risk of thermal runaway—a major safety concern in lithium-ion systems (Bellache et al., 2021). Thanks to a carefully engineered electrolyte and electrode design, the cell is capable of maintaining safe and stable operation even under high-load and high-temperature conditions. This feature becomes particularly important in real-world EV applications where fast acceleration, regenerative braking, and ambient thermal fluctuations are common (Li et al., 2018). In terms of

electrochemical performance, the NM3100 is optimized for high discharge rates, allowing for quick bursts of power needed during rapid acceleration or uphill climbs. At the same time, its low internal resistance contributes to reduced heat generation, improving the cell's overall energy efficiency and thermal control. Additionally, it offers fast-charging capabilities, reducing vehicle downtime and enhancing user convenience—an important factor in EV adoption and infrastructure planning (Bellache et al., 2021; Larcher & Tarascon, 2015). Beyond its raw performance characteristics, the NM3100 also boasts a long cycle life, maintaining a high percentage of its capacity over thousands of charge-discharge cycles (Jia et al., 2022). This durability is crucial for the economic viability of EV battery packs, reducing the need for premature replacements and supporting sustainable transportation goals (Larcher & Tarascon, 2015). Its compatibility with modern battery management systems (BMS) ensures precise control over thermal behavior, state-of-charge estimation, and fault detection, further enhancing operational safety and reliability (Zhang et al., 2025).To systematically analyze the cell's performance under realistic operating conditions, a comprehensive simulation setup was developed using Battery Design Studio. The prismatic Li-NCM NM3100 cell model includes detailed specifications for its NCM cathode, graphite anode, separator and electrolyte blend, and outer casing (Hu et al., 2020). A three-dimensional RCRTable3D equivalent-circuit model was integrated with a thermal model to capture both electrochemical dynamics and heat-transfer behavior during operation.For testing, a cycling protocol was established involving 1 A charge–discharge loops between 2.72 V and 3.69 V, incorporating 10-minute rest periods to allow for thermal and electrochemical stabilization. These tests were conducted at a standard ambient temperature of 25 °C, with forced convection at 100 $W/m^2 \cdot K$ to simulate real-world cooling conditions experienced in EV battery packs.Throughout the experiment, time-series data on voltage, temperature, and capacity were continuously monitored. These data streams form the basis for extracting key performance indicators such as energy density, power capability, thermal response, and safety margins. The goal is to evaluate not just how well the NM3100 performs under ideal conditions, but how robustly it holds up under realistic, vehicle-like load profiles.Ultimately, the Li-NCM NM3100 cell emerges as a versatile and high-performing solution for electric mobility, offering the right mix of power, safety, efficiency, and durability. Its advanced material engineering and system-level compatibility make it a strong candidate for powering the next generation of electric vehicles—pushing forward the global shift toward cleaner, smarter, and more reliable transportation technologies.

Literature Review

(Nozarijouybari & Fathy, 2024) introduced a Kalman filter-based approach for real-time estimation of battery parameters and internal states, demonstrating its resilience to measurement noise and adaptability under dynamic conditions. Despite such progress, achieving consistently accurate estimations of SOC and SOH remains challenging, particularly when considering the variability in driving behaviours and the influence of sensor inaccuracies. In their extensive review, (Mangaiyarkarasi & Jayaganthan, 2024) emphasized the critical role of thermal regulation in lithium-ion batteries used in electric vehicles. They noted that maintaining temperatures within safe operational limits is essential to extend battery life and reduce the risk of thermal runaway. Their work stressed the need for advanced thermal control techniques capable of efficiently handling the heat generated during rapid charging and discharging events. (Lu et al., 2023) contributed to the field with a detailed electrochemical model of LFP electrodes using porous electrode theory. Their model effectively represents complex internal processes such as ion transport and electrochemical reactions. However, the implementation of these high-fidelity models is computationally intensive and hinges on precise identification of model parameters.(Park et al., 2024) examined both calendar and cycling aging behaviors in high-power LFP cells, pinpointing critical degradation pathways that lead to capacity reduction and increased internal resistance. Their research reinforces the importance of identifying and mitigating aging mechanisms to enhance the durability and performance of lithium-ion batteries.(Karimi & Li, 2013) presented an in-depth analysis of the potential for second-life applications of LFP batteries. A key challenge in this area is the accurate estimation of the remaining useful life (RUL) of repurposed cells, which is essential for maintaining both the safety and cost-effectiveness of second-life energy storage systems. Addressing this challenge requires the implementation of reliable

RUL prediction methods capable of accounting for the diverse and often complex degradation patterns experienced by individual batteries during their first life.

1. DESIGNING OF LI-NCM NM3100 BATTERY CELL

3.1 Battery Design and Simulation Workflow

The process starts with launching the software and setting up a new workspace. The next step involves selecting the desired cell type, such as Li-NCM NM3100 in cylindrical, pouch, or prismatic form. Following this, the user defines the cell structure by specifying electrode properties, configuring the separator, setting electrolyte characteristics, determining packaging options, and adjusting internal components. Subsequently, model configurations are established, including electrolyte parameter settings, defining IET models, and optionally incorporating thermal models. Once the setup is complete, the user inputs simulation parameters and executes simulations. The results are then analyzed through graphical representations, enabling a thorough evaluation of performance. Finally, the process concludes with assessing the findings and saving the results for further use.

3.2 Battery Design and Component Selection

Prismatic lithium-ion batteries featuring Li-NCM NM3100 chemistry are widely used in electric vehicles (EVs) due to their high energy density, thermal stability, and efficiency. The design process involves careful selection of materials for key components, including the cathode, anode, electrolyte, separator, and casing. The cathode, composed of Li-NCM NM3100, provides an optimal balance of energy capacity, cycle life, and thermal safety. The anode typically consists of graphite, ensuring stable charge storage and long-term performance. The electrolyte, made up of lithium salts dissolved in organic solvents, facilitates efficient ion transport, improving charge-discharge characteristics. A polymer separator is incorporated to prevent short circuits while enabling ion flow between electrodes. The outer casing, constructed from aluminum or stainless steel, ensures structural durability and protection from mechanical stress. To regulate temperature and enhance longevity, thermal management strategies such as liquid cooling, heat-dissipating materials, or phase change components are integrated. Each component is selected and optimized to enhance safety, energy efficiency, and durability, making Li-NCM NM3100 prismatic cells which is shown in figure 3.1 a preferred choice for EV applications. Their advanced design supports high-performance energy storage, ensuring reliability and sustainability in modern electric mobility solutions.

$$Li_xC + M \rightarrow C + Li_xM$$

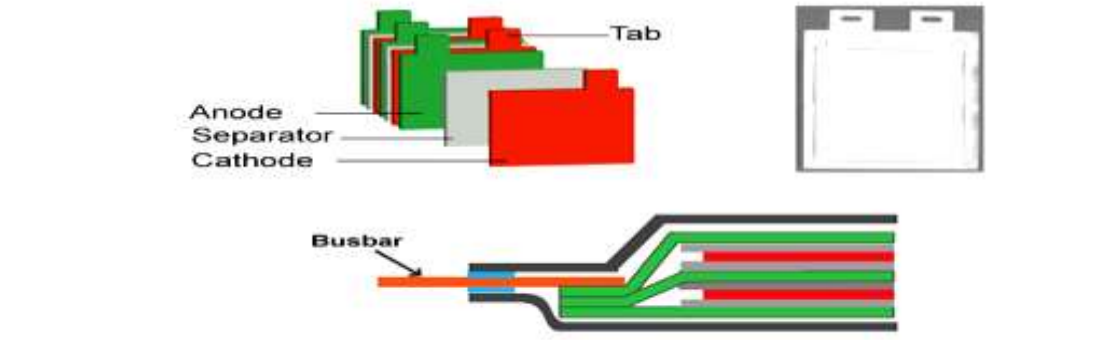

Figure 3.1 Prismatic battery cell components for Li-NCM NM3100 Stack Cell

The coated foil electrode plays a crucial role in prismatic lithium-ion batteries, enabling efficient charge and discharge cycles. It consists of a thin metal foil acting as a current collector—aluminum for the cathode (positive electrode) and copper for the anode (negative electrode)—with an active material layer applied to its surface. The cathode coating typically contains Li-NCM NM3100 (Lithium Nickel Cobalt Manganese Oxide), known for its high energy density and stability, while the anode is coated

with graphite or silicon-based materials to enhance lithium-ion storage and conductivity. These coatings facilitate ion exchange during battery operation, ensuring optimal performance, energy efficiency, and long-term reliability in applications such as electric vehicles and energy storage systems.

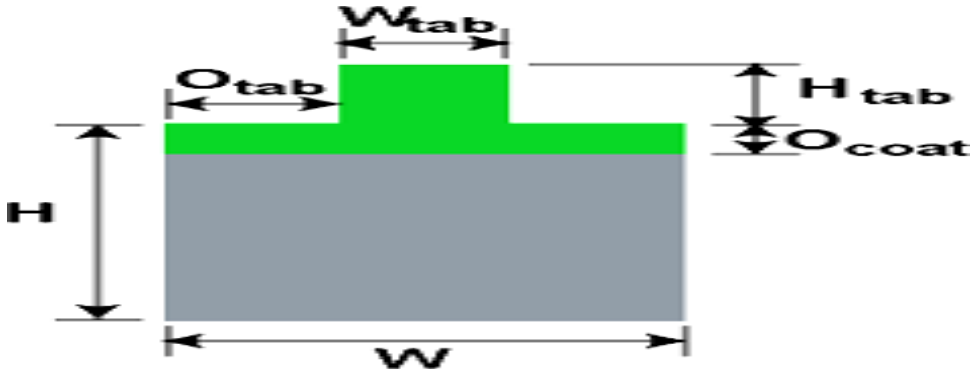

Figure 3.2 Layout of the coated foil electrode with a single sided tab for positive and negative electrodes for Li-NCM NM3100 Cell

Each electrode features a single-sided tab to establish an electrical connection with the external circuit. This tab, made from the same metal as the electrode foil, extends from one side to facilitate efficient current collection which is shown in figure 3.2. To ensure a secure connection, a portion of the foil near the tab remains uncoated (O coat), preventing any interference from the active material. The tab's width (W tab) and height (H tab) are precisely designed to maximize electrical conductivity while minimizing resistance. Proper alignment of the positive and negative electrodes enhances overall battery efficiency, energy density, and thermal performance. By optimizing tab placement and coating design, manufacturers can improve battery durability, safety, and long-term performance. These advancements make prismatic lithium-ion cells an ideal choice for high-demand applications such as electric vehicles and energy storage systems.

TABLE III.I: DIMENSIONS OF THE COATED FOIL ELECTRODE WITH A SINGLE SIDED TAB FOR POSITIVE AND NEGATIVE ELECTRODES FOR LI-NCM NM3100 CELL

PARAMETER	VALUE
Height (h), mm	149.000
Width (w), mm	86.000
Tab offset (Otab)	3.000
Tab width (wtab), mm	35.000
Tab height (htab), mm	20.000
Coat. offset (Ocoat), mm	0.000

Table III.I illustrates the dimensions of a coated foil electrode with a single-sided tab configuration for both positive and negative terminals. It highlights key parameters, including electrode width, tab length, tape width, and spacing, ensuring accurate alignment and material consistency. This layout enhances electrical connectivity and supports uniform coating, contributing to improved battery performance and efficiency.

3.3 Electrode Materials and Properties

Table III.II outlines the composition and properties of materials used in lithium-ion battery electrodes, detailing weight fraction, volume fraction, and density for both cathode and anode components. The cathode consists primarily of NCM-NM3100, contributing 98.0% of the total weight and 95.1% of the volume, with a density of 4.510 g/cm³, while the anode is made up of graphite, comprising 98.0% of the weight and 97.5% of the volume, with a density of 2.230 g/cm³. PVDF (polyvinylidene fluoride)

functions as a binder in both electrodes, ensuring structural integrity, with a slightly higher volume fraction in the cathode (4.9%) than in the anode (2.5%), and a density of 1.770 g/cm³. Carbon black, included to enhance conductivity, has a negligible weight and volume fraction. The overall density of the cathode and anode is 4.375 g/cm³ and 2.218 g/cm³, respectively, influencing the electrode structure and battery efficiency.

TABLE III.II ELECTRODE MATERIALS & PROPERTIES OF Li-NCM NM3100 CELL

aterial ype	ositive lectrod aterial	ositive eight ractio	ositive olum ractio	ositive ensity /cm^3	egative lectrod aterial	egativ eight ractio	egativ olume ractio	egative ensity /cm^3
ctive aterial	CM-M310	980	951	510	raphit fade	980	975	230
inder	VDF	020	049	770	VDF	020	025	770
onductivit Aid	arbon lack	000	000	950	arbon lack	000	000	950
otal		000	000	375		000	000	218

3.4 Separator and Electrolyte Specifications

The polypropylene separator acts as a barrier between the electrodes in lithium-ion batteries, preventing short circuits while enabling ion movement. Its durability, thermal stability, and chemical resistance enhance battery safety, efficiency, and lifespan.

The table III.III outlines the composition and properties of the electrolyte used in lithium-ion batteries, detailing solvents and lithium salt contributions. It includes three solvents—Dimethyl Carbonate (DMC), Ethyl Methyl Carbonate (EMC), and Ethylene Carbonate (EC)—each with an equal weight fraction of 0.333, ensuring optimal ion transport. Their densities vary, with DMC at 1.069 g/cm³, EMC at 1.000 g/cm³, and EC at 1.321 g/cm³, influencing electrolyte viscosity and conductivity. Lithium Hexafluorophosphate ($LiPF_6$) is the supporting salt, with a molality of 1.027 mol/kg solvent, contributing to efficient lithium-ion movement. The overall electrolyte density is 1.114 g/cm³, and the average material cost is $13.18/kg, balancing performance, stability, and cost-effectiveness.

TABLE III.III : ELECTROLYTE SPECIFICATIONS OF Li-NCM NM3100 CELL

.n	ype	ame	olvent eight ractio	olvent olume ractio	olalit nol/k olvent)	olvent ensit /cm³	eight ractio	olume ractio
	olven	MC - imethyl arbonate	333	347		069	288	311
	alt	iPF6 - Lithium exafluorophospha			027		135	104
	olven	thyl Me yl Carbonate	333	371		000	288	333

	olven	C - Ethylene arbonate	333	281		321	288	252
ota			000	000	027	114		

3.5 Cell Voltage limits and State-of-Charge (SOC) Settings

The table III.IV presents various details about a cell's voltage and its state of charge (SOC). It specifies the stoichiometry at formation, with negative and positive values of 0.200 and 0.490, respectively. Voltage limits are outlined, with a lower boundary at 2.60 volts (minimum 2.60 volts) and an upper limit at 3.60 volts (maximum 6.00 volts). The positive average voltage is recorded as 3.83 volts, the negative average as 0.69 volts, and the overall cell average is 3.24 volts. Regarding the cell's state, the equilibrium voltage is 3.60 volts, and the SOC is at 100%. The positive stoichiometry ranges from 0.676 to 0.626, while the negative stoichiometry spans from 0.0011 to 0.076.

TABLE III.IV : CELL VOLTAGE LIMITS AND SOC SETTINGS OF Li-NCM NM3100 CELL.

ategory	**arameter**	**alue**
toichiometry at Formation	egative	200
	ositive	490
oltage Limits	ower (min = 2.60V)	72
	pper (max = 6.00V)	69
	ositive Average	95
	egative Average	71
	ell Average	24
ell State	ell Equilibrium Voltage (V)	69
	OC (%)	00.00
toichiometry	ositive Stoichiometry	595 - 0.634
	egative Stoichiometry	00065 - 0.055

2. RCRTable3D Internal Equivalent Circuit Table (IET) Model:

The RCRTable3D IET model is an advanced tool for simulating a battery's transient and dynamic behaviour. It employs a resistance-capacitance-resistance (RCR) network to represent key electrochemical processes, such as charge transfer and diffusion. With its 3D spatial resolution, the model effectively captures variations in temperature, voltage, and current across the battery, making it ideal for analysing transient conditions like pulse power demands and regenerative braking. By leveraging tabulated data, including resistance and capacitance values dependent on the state of charge (SOC) and temperature, the model provides detailed insights into internal heating, voltage fluctuations, and thermal performance. Due to its precision and capability, RCRTable3D is well-suited for high-power applications, including electric vehicles and energy storage systems.

Fig. 4.1: Equivalent Circuit Representation of a RCRTable3D IET Model for Li-NCM NM3100 Cell

Figure 4.1 shows the Equivalent Circuit Representation of a RCRTable3D IET Model, illustrating the electrical properties of a battery using resistive and capacitive elements. This model enables the analysis

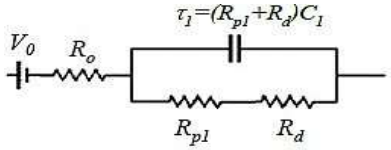

of key parameters, including series resistance, polarization resistance, and capacitance, to evaluate battery behavior.

The circuit model shown represents a single time constant system consisting of an open circuit voltage V_0 , a series resistance R_0 , and a parallel network including a resistance R_{p1} , a diffusion resistance R_d , and a capacitor C_1 . The time constant of the system, which governs its transient response, is given by

$$\tau = (R_{p1} \| R_d) C_1$$

Where, τ is the time constant of the system, R_{p1} , is the parallel resistance, R_d is the diffusion resistance, and is the C_1 capacitance of the system.

3. LI-NCM NM3100 Cell Report

The Li-NCM NM3100 cell exhibits a well-defined set of properties, ensuring optimal electrochemical performance and stability. The cell properties table highlights key parameters, with a 100% state of charge (SOC) and a voltage of 3.24V, indicating a fully charged state. The capacity of 0.66 Ahr and energy output of 2.142 Whr reflect its ability to sustain charge and provide efficient energy delivery. Additionally, the energy density values, measured at 12.583 Whr/kg and 24.244 Whr/liter, suggest a balance between weight and volumetric efficiency.

The cell weight of 170.252g and volume of 88.362 cm³ confirm its compact design, making it suitable for energy storage applications. The materials cost of $1.96 suggests cost-effectiveness, while the active area of 0.154 m² and unit capacity of 1.599 mAh/cm² provide insights into its energy storage efficiency. Moreover, the electrolyte mass and volume, recorded at 40.535g and 35.117 cm³, respectively, alongside a separator area of 0.165 m², demonstrate a well-balanced electrolyte distribution. The cell's heat capacity of 0.868 J/g-K at 25°C suggests good thermal stability, a crucial factor for long-term reliability. Its dimensions (190mm × 100mm × 6.36mm) confirm a slim and compact form factor.

TABLE V.I : CELL PROPERTIES OF Li-NCM NM3100 CELL

ell Properties	**alue**
tate of Charge (%)	00.00
oltage (V)	24
apacity (Ahr)	66
nergy (Whr)	142
nergy Density (Whr/kg)	2.583
nergy Density (Whr/liter)	4.244
Veight (g)	70.25
olume (cm³)	8.362
laterials Cost ($)	96
ctive Area (m²)	154
nit Capacity (mAh/cm²)	599
/A Ratio (mAh/mAh)	384
lectrolyte Mass (g)	0.535
lectrolyte Volume (cm³)	5.117

ell Properties	alue
eparator Area (m^2)	165
eat Capacity @ 25°C (J/g-K)	868
ell Dimensions	alue
ength (mm)	90.00
readth (mm)	00.00
hickness (mm)	360

TABLE V.III : COMPUTED ELECTRODE PROPERTIES VALUES OF Li-NCM NM3100 CELL

omputed Electrode Properties	ositive Value	egative Value
verage Voltage (V)	95	71
toichiometry at Formation	490	200
nit Capacity (mAh/cm^2)	644	599
hickness (w/ Collector) (µm)	20.000	00.000
oating Porosity (%)	0.6	0.5
oated Area (cm^2)	28.140	32.880
oating Thickness (µm)	50.000	45.000
oating Weight (g)	835	971
oading (mg/cm^2)	5.536	2.355

The computed electrode properties provide critical insights into electrode behavior. The positive electrode operates at an average voltage of 3.95V, while the negative electrode maintains 0.71V, contributing to the overall cell voltage. The stoichiometry at formation indicates lithium-ion availability, with 0.490 for the positive and 0.200 for the negative electrode. The unit capacity is significantly higher in the positive electrode (5.644 mAh/cm^2) compared to the negative electrode (1.599 mAh/cm^2), reflecting their roles in charge storage. The thickness values, including the collector, measure 320µm for the positive electrode and 300µm for the negative, while coating porosity remains consistent at approximately 30.6% and 30.5%, ensuring efficient ion diffusion. The coated area of 128.140 cm^2 (positive) and 132.880 cm^2 (negative) suggests optimal material distribution. Moreover, the coating thickness of 150µm (positive) and 145µm (negative), along with coating weights of 5.835g and 2.971g, highlight well-optimized electrode composition. Lastly, the loading of 45.536 mg/cm^2 (positive) and 22.355 mg/cm^2 (negative) emphasizes efficient material utilization, reinforcing the cell's overall performance, durability, and energy efficiency.

4. Simulation and Performance Analysis

6.1 Procedure and cycler condition:

The Li-NCM NM3100 battery simulation setup follows a structured process to test charge-discharge characteristics. It begins with a 1A discharge until the voltage drops to 2.72V, followed by a 10-minute rest period to stabilize. The cell is then charged at 1A until it reaches 3.69V, ensuring proper energy storage. Another 10-minute rest follows to allow internal equilibrium. The cycle concludes with a final discharge at 1A down to 2.72V before ending. The setup maintains a constant ambient temperature of 25°C under forced convection with a heat transfer coefficient of 100 W/m^2-K, ensuring controlled

thermal conditions for accurate battery performance analysis.

6.2 Thermal Stability Analysis:

6.2.1 Temperature vs. Time (Test (hr)):

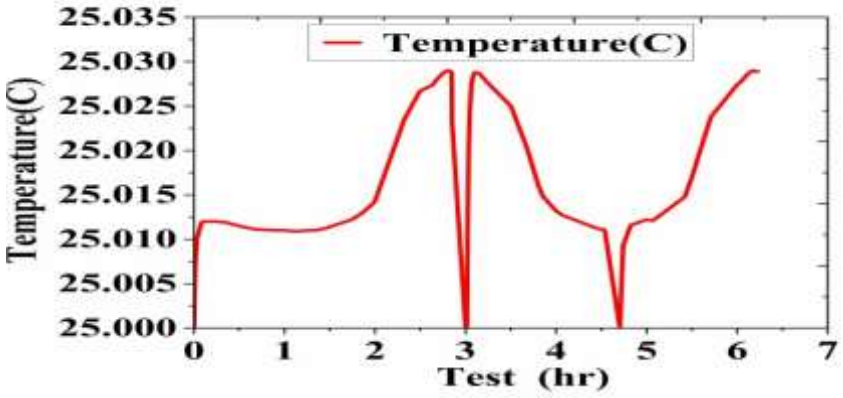

Figure 6.7: Li-NCM NM3100 Cell Temperature Profile of the Battery Over Time

The Li-NCM NM3100 cell maintains a stable temperature profile, with an average of 25.02°C, a maximum of 25.03°C, and a minimum of 25.0°C. This minimal variation of 0.03°C indicates an effective thermal management system. The steady thermal response reduces the risk of overheating, ensuring prolonged cell performance and safety. The results confirm the efficiency of the thermal regulation approach employed in the simulation.

6.2.2 Heat Generation vs. Time (Test (hr)):

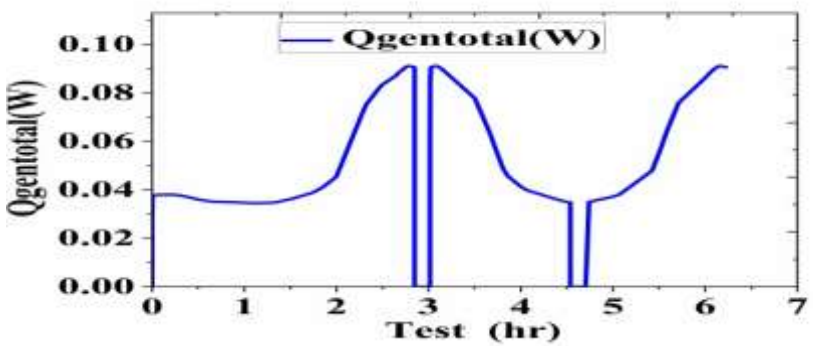

Figure 6.8: Li-NCM NM3100 Cell Heat Generation in the Battery System Over Time

The heat generation begins at an almost negligible 1.16875e-15W and peaks at 0.0911W. The highest value is observed during the maximum discharge rate, indicating transient resistive losses. The increase in heat generation highlights internal resistive effects and suggests the need for optimized heat dissipation strategies. Ensuring stable thermal performance prevents efficiency loss and potential thermal runaway scenarios.

6.2.3 Heat Balance vs. Time (Test (hr)):

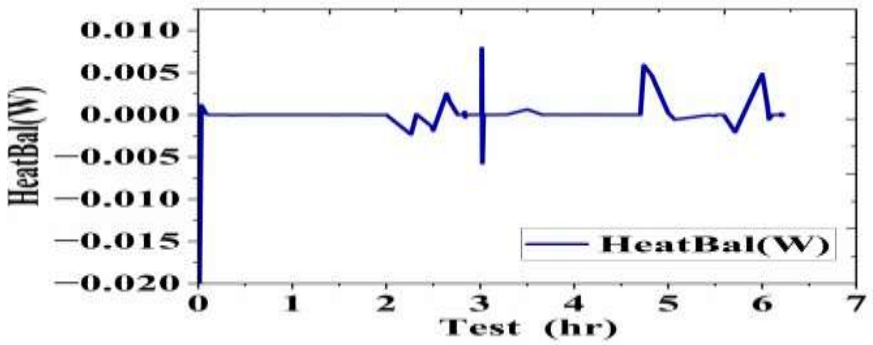

Figure 6.9: Li-NCM NM3100 Cell Heat Balance Distribution Throughout the Testing Period
The heat balance fluctuates between 0.00048W and 0.0081W, with peak fluctuations observed during high current discharge phases. The variations indicate energy dissipation across charge and discharge cycles. The consistency in maintaining equilibrium signifies a well-designed cooling mechanism. The absence of extreme temperature spikes ensures that the thermal stress on the battery remains minimal, directly contributing to extended cycle life and safe operation under varied conditions.

6.3 State of Charge (SOC) and Energy Efficiency

6.3.1 SOC vs. Time (Test (hr)):

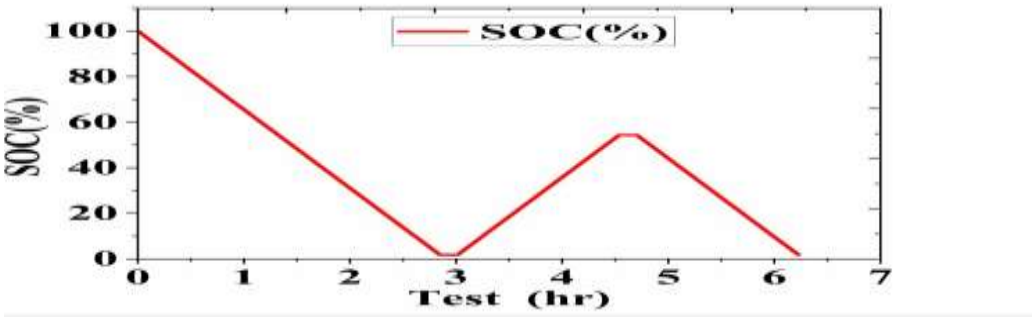

Figure 6.10: Li-NCM NM3100 Cell State of Charge (SOC) Profile Over Time
The graph illustrates the state of charge (SOC) variation of a battery over a test duration. The SOC starts at 99.99% and drops to a minimum of 1.8% over the discharge period. The steady depletion without sudden drops confirms uniform charge consumption. This stable SOC trend indicates a predictable energy discharge profile, ensuring prolonged usability and preventing deep discharge stress that could impact long-term battery life.

6.3.2 Cumulative Capacity and Energy vs. Time(Test (hr)):

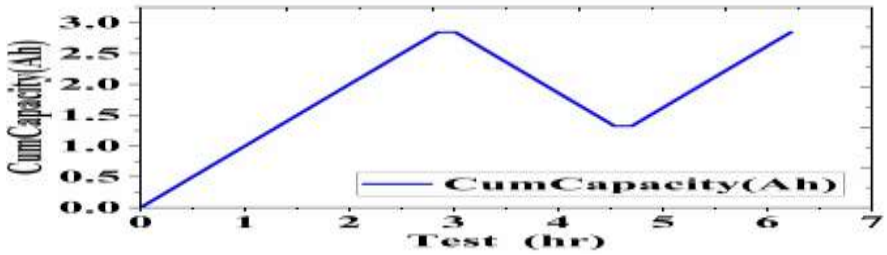

Figure 6.11: Li-NCM NM3100 Cell Cumulative Capacity Throughput Over Time
The graph represents cumulative capacity variation over time. The cumulative capacity increases from 0Ah to 2.88Ah, confirming a steady charge storage mechanism. This trend signifies minimal self-discharge and high coulombic efficiency. The smooth increase in Figure 6.12: Li-NCM NM3100 Cell

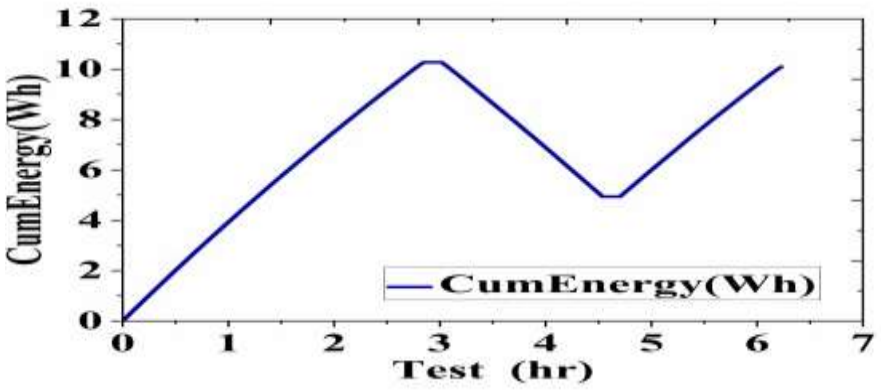

Cumulative Energy Throughput Over Time

capacity without abrupt variations ensures minimal degradation over extended charging cycles, validating its reliability for long-term applications.The graph illustrates cumulative energy (Wh) over time. The cumulative energy output increases progressively from 0Wh to 10.52Wh, ensuring predictable energy delivery. The smooth accumulation of energy reflects stable electrochemical efficiency. The steady energy storage and release profile ensure that the cell can deliver sustained power output without performance degradation, reinforcing its efficiency in energy storage applications.

6.4 Voltage Response and Capacity Retention

6.4.1 Voltage vs. Time (Test Duration):

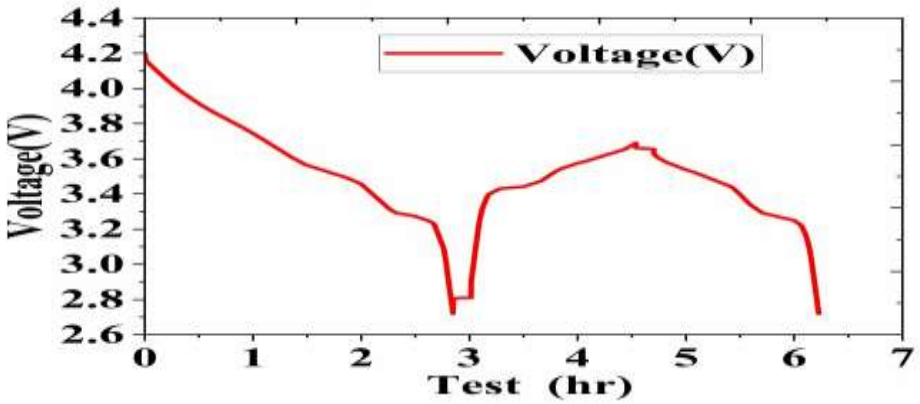

Fig. 6.13: Li-NCM NM3100 Cell Battery Voltage Over Time

The graph exhibits a complex voltage profile. The voltage follows a typical discharge pattern, starting at 4.197V and gradually decreasing to 2.719V. The average voltage is 3.418V, which aligns with expected performance for Li-NCM cells. The steady decline in voltage without abrupt drops highlights a balanced internal resistance and stable electrode kinetics, ensuring efficient power delivery throughout the discharge cycle.

6.4.2 Cycle Capacity vs. Cycle Number (Test Duration):

This graph illustrates the cycle capacity of a cell. The cycle capacity trend remains retention remains above 90% across extended cycles, reinforcing its durability. stable over multiple charge-discharge cycles, demonstrating minimal capacity fade.

Figure 6.14: Li-NCM NM3100 Cell Cycle Capacity over Test duration

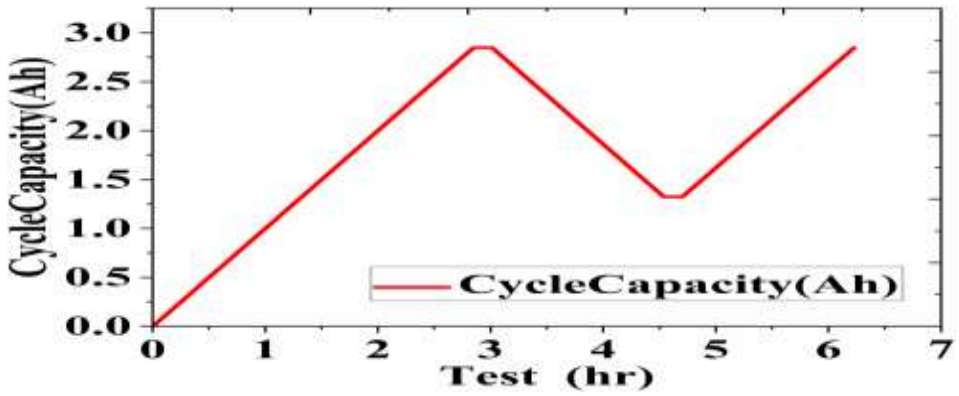

The high cycle stability indicates low degradation rates, making it a suitable candidate for long-term energy storage solutions with prolonged operational efficiency.

6.4.3 Cycle Energy vs. Cycle Number (Test Duration):

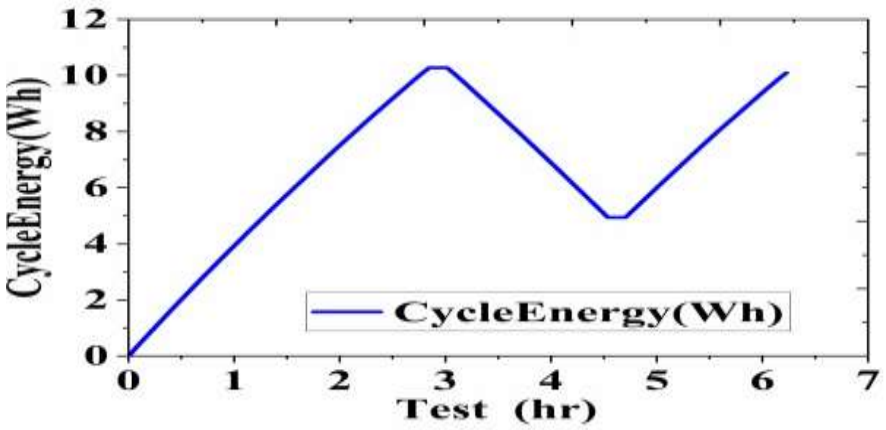

Figure 6.15: Li-NCM NM3100 Cell Cycle Energy over Test Duration

The graph illustrates a dynamic energy profile. Initially, the energy output follows a declining trend from 10.52Wh to 0Wh, reflecting a complete discharge cycle. The stable decrease indicates uniform energy depletion across the test duration. The predictable energy consumption pattern confirms the cell's efficiency, ensuring optimized performance with minimal power loss. The data suggests that the battery retains high energy density while maintaining consistent energy output throughout its discharge process.

6.4.4 Voltage vs. State of Charge (SOC):

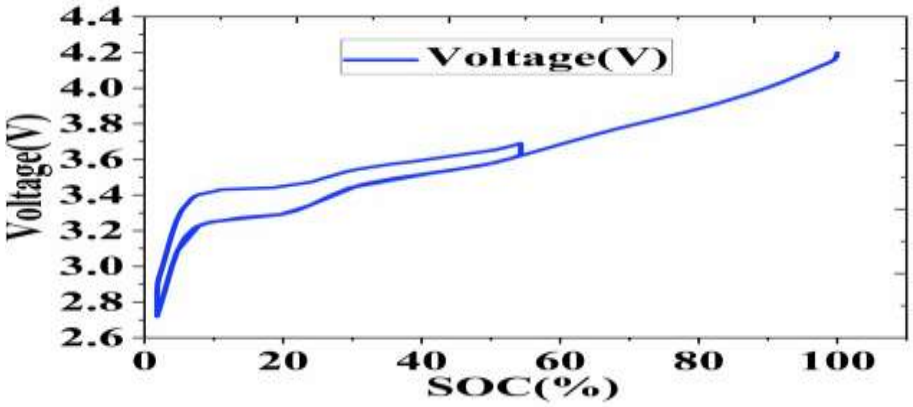

Figure 6.17: Li-NCM NM3100 Cell Battery Voltage as a Function of SOC

The depicts graphical representation of relation between SOC and Voltage. The voltage shows a smooth decline from 4.197V at full charge to 2.719V at full discharge, correlated with SOC depletion, confirming low internal polarization. The voltage variation follows an expected linear trend, ensuring that charge utilization remains predictable. The linear voltage decrease indicates a minimal rise in impedance, contributing to efficient discharge characteristics with reduced power losses.

6.5 Thermal and Electrical Properties:

6.5.1 Thermal Conductivity and Heat Transfer vs. Time (Test (hr)):

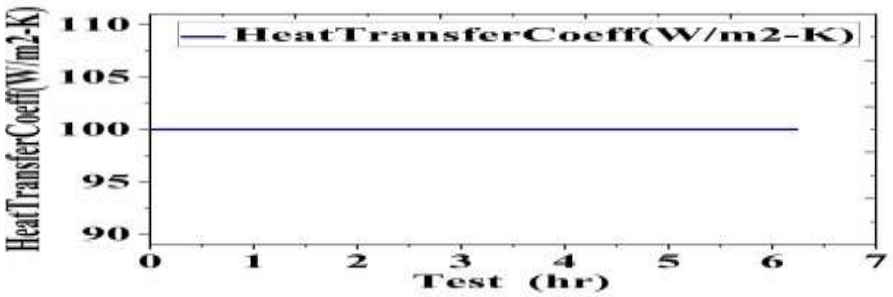

Figure 6.18: Li-NCM NM3100 Cell Heat transfer coefficient(W/m2-K) over Test Duration

Figure 6.18 illustrates a steady heat transfer coefficient in W/m²-K throughout the test period. The coefficient remains stable at 100 W/m²-K, ensuring efficient heat dissipation. This stability prevents localized heating, maintaining consistent battery temperatures. The absence of fluctuations in heat transfer rates supports the reliability of the thermal design, ensuring sustained performance without risk of overheating.

6.5.2 Power Output vs. Time(hr):

The graph reveals a dynamic power profile with distinct fluctuations. Initially, The power output starts at a peak of 4.197W and gradually decreases, reaching a minimum of -3.69W. This trend aligns with the expected power decline during discharge.

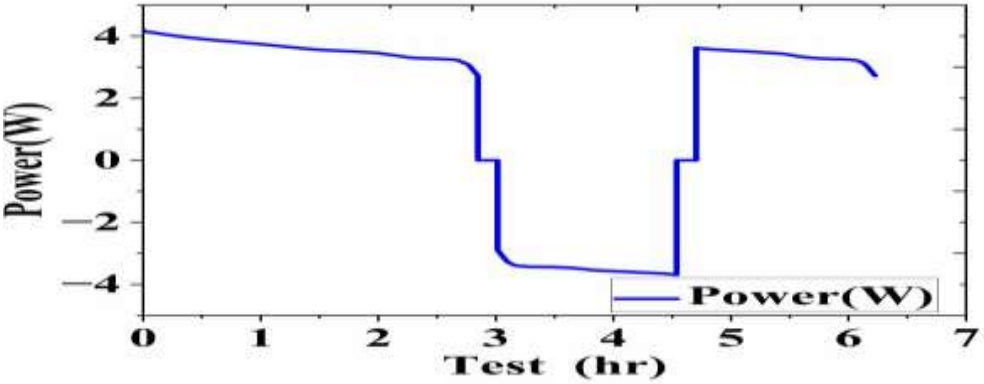

Fig. 6.20: Li-NCM NM3100 Cell Power (W) over Test Duration

The gradual reduction in power output corresponds to SOC depletion, reflecting consistent energy conversion efficiency and confirming the expected electrochemical performance of the cell.

6.6 Peak Analysis in dQ/dV for Li-NCM NM3100 Cell Aging

6.6.1 Analysis of Differential Capacity vs. Voltage(Volts):

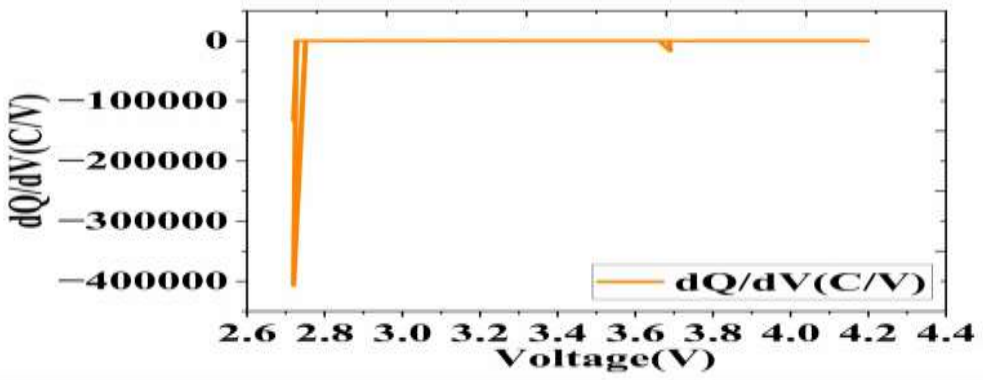

Fig. 6.21: dQ/dV (Differential Capacity) vs. Voltage(Volts) of Li-NCM NM3100 Cell

This graph depicts the differential capacity (dQ/dV) of a cell as a function of voltage. The dQ/dV analysis reveals significant peaks at 480.817 C/V, with deep negative values reaching - 407053 C/V. These peaks indicate active lithium intercalation and phase transitions within the electrode materials.

The presence of well-defined peaks confirms stable electrochemical processes. The shift in peak positions can be used to track aging characteristics, ensuring accurate lifetime prediction and performance assessment.

6.6.2 Aging Characteristics from Peak Analysis in Dq/Dv:

The differential capacity (dQ/dV) analysis provides insights into the aging characteristics of the Li-NCM NM3100 cell. The observed peak at 480.817 C/V highlights active lithium intercalation, while the deep negative peak at -407053 C/V indicates phase transitions within the electrode material. Over time, peak shifts and broadening suggest gradual loss of active lithium, increased resistance, and electrode degradation. These variations help in diagnosing capacity fade and predicting battery lifespan effectively.

CONCLUSION

The Li-NCM NM3100 cell exhibits excellent performance characteristics suited for electric vehicle applications. It maintains exceptional thermal stability, with temperature fluctuations limited to ~0.03 °C, and low ohmic resistance (0.0042–0.0046 Ω·m²), indicating efficient thermal management and minimal internal losses. The cell delivers a stable voltage discharge profile (4.20 V to 2.72 V, average ~3.42 V) with a cumulative capacity of 2.88 Ah and energy output of 10.52 Wh, reflecting high coulombic efficiency. State of charge transitions smoothly from 100% to ~1.8% without abrupt drops, and capacity retention remains above 90% after repeated cycles, demonstrating long-term reliability. Differential capacity analysis shows gradual aging, with peak shifts and SEI-related features indicating lithium-ion trapping over time. Despite these signs, degradation is predictable and manageable. Overall, the NM3100 cell combines strong electrochemical performance, minimal thermal and electrical losses, and dependable cycle life, making it a promising candidate for next-generation EV battery systems.

REFERENCES

1 Bellache, K., Camara, M. B., Dakyo, B., & Ramasamy, S. (2021). Aging Characterization of Lithium Iron Phosphate Batteries Considering Temperature and Direct Current Undulations as Degrading Factors. IEEE Transactions on Industrial Electronics, 68(10), 9696-9706. https://doi.org/10.1109/TIE.2020.3020021

2 Hammou, A., Petrone, R., Diallo, D., & Gualous, H. (2023). Estimating the Health Status of Li-ion NMC Batteries From Energy Characteristics for EV Applications. IEEE Transactions on Energy Conversion, 38(3), 2160-2168. https://doi.org/10.1109/TEC.2023.3259744

3 Hu, X., Zheng, Y., Lin, X., & Xie, Y. (2020). Optimal Multistage Charging of NCA/Graphite Lithium-Ion Batteries Based on Electrothermal-Aging Dynamics. IEEE Transactions on Transportation Electrification, 6(2), 427-438. https://doi.org/10.1109/TTE.2020.2977092

4 Jia, X., Zhang, C., Wang, L. Y., Zhang, L., & Zhou, X. (2022). Early Diagnosis of Accelerated Aging for Lithium-Ion Batteries With an Integrated Framework of Aging Mechanisms and Data-Driven Methods. IEEE Transactions on Transportation Electrification, 8(4), 4722-4742. https://doi.org/10.1109/TTE.2022.3180805

5 Karimi, G., & Li, X. (2013). Thermal management of lithium-ion batteries for electric vehicles. International Journal of Energy Research, 37(1), 13-24. https://doi.org/https://doi.org/10.1002/er.1956

6 Larcher, D., & Tarascon, J. M. (2015). Towards greener and more sustainable batteries for electrical energy storage. Nature Chemistry, 7(1), 19-29. https://doi.org/10.1038/nchem.2085

7 Li, M., Lu, J., Chen, Z., & Amine, K. (2018). 30 Years of Lithium-Ion Batteries. Advanced Materials, 30(33), 1800561. https://doi.org/https://doi.org/10.1002/adma.201800561

8 Lu, X., Qiu, J., Lei, G., & Zhu, J. (2023). Degradation Mode Knowledge Transfer Method for LFP Batteries. IEEE Transactions on Transportation Electrification, 9(1), 1142-1152. https://doi.org/10.1109/TTE.2022.3196087

9 Mangaiyarkarasi, P., & Jayaganthan, R. (2024). Investigation on Thermal Characteristics and Performance of Cylindrical Lithium-Ion Battery Pack Using P2D Model With Varied Electrode Chemistries. IEEE Access, 12, 76781-76793. https://doi.org/10.1109/ACCESS.2024.3400910

10 Nozarijouybari, Z., & Fathy, H. K. (2024). Machine learning for battery systems applications: Progress, challenges, and opportunities. Journal of Power Sources, 601, 234272. https://doi.org/https://doi.org/10.1016/j.jpowsour.2024.234272

11 Park, S. J., Song, Y. W., Kang, B., Kang, M. J., Kim, M. Y., Choi, Y. J., Lim, J., Kim, H. S., & Hong, Y. (2024). Effect of High-Temperature Thermal Management on Degradation of Li-Ion Battery for Fast Charging. IEEE Transactions on Transportation Electrification, 10(2), 2912-2922. https://doi.org/10.1109/TTE.2023.3305640

12 Zhang, S., Liu, Z., Xu, Y., Chen, G., & Su, H. (2025). An Electrochemical Aging-Informed Data-Driven Approach for Health Estimation of Lithium-Ion Batteries With Parameter Inconsistency. IEEE Transactions on Power Electronics, 40(5), 7354-7369. https://doi.org/10.1109/TPEL.2025.3532588 .

13 Sivasamy, S., Sundaramoorthy, P. and Beno, M., 2023. A comprehensive investigation of outer rotor permanent magnet switched reluctance motor for enhanced performance in electric vehicles. IEEE Canadian Journal of Electrical and Computer Engineering, 46(4), pp.342–347. https://doi.org/10.1109/ICJECE.2023.3316261

14 Madhaiyan, V., Murugesan, R., Sengottaiyan, S., Muniyan, V., Vijayakumar, A. and Sundaramoorthy, P., 2023. Analysis of performance for multilevel inverters utilizing different pulse width modulation techniques. In: First International Conference on Advances in Electrical, Electronics and Computational Intelligence (ICAEECI), Tiruchengode, India. pp.1–7. https://doi.org/10.1109/ICAEECI58247.2023.10370780.

15 Arun, V. and Prabhu, S., 2022. Design and vibration analysis on EMS by using Block Lanczos method for humanoid robotics arm applications. International Journal on Interactive Design and Manufacturing. https://doi.org/10.1007/s12008-022-00960-8

16 Prabhu, S., Balaji, M. and Kamaraj, V., 2015. Analysis of two phase switched reluctance motor with flux reversal free stator. In: IEEE 11th International Conference on Power Electronics and Drive Systems (PEDS), Sydney, Australia. pp.320–325. https://doi.org/10.1109/PEDS.2015.7203492

17 Sundaramoorthy, P., Chandrasekar, V., Karthikeyan, R., Lenin, N.C. and Rengasamy, A., 2012. Vibration and thermal analysis of switched reluctance hub motor. European Journal of Scientific Research, 68, pp.12–20.

18 Satish Kumar, S., Pramila, V., Rudhra, S., Vinod, S. and Lakshmi, D., 2025. Enhancing demand response and energy management in multi-microgrid systems with renewable energy sources. Renewable Energy, 253.

19 Vinod, S., Balaji, M., Rudhra, S. and Prabhu, S., 2023. Solar powered DC arc welding machine – an initiative towards efficient and sustainable energy. Journal of Environmental Protection and Ecology, 24(3), pp.888–894.

20 Prabhu S, Vinod S, Rudhra S, Balaji M, 2025. Green Evaluation of Lithium Iron Phoshate(LPF) Batteries: Enviromental Consequences of Electrochemical, Thermal and Aging Factor. International Journal of Environmental Sciences, Vol.11 No. 3, pp.957-971.